European Polymer Journal 166 (2022) 111027

Contents lists available at ScienceDirect

European Polymer Journal

journal homepage: www.elsevier.com/locate/europolj

Hyaluronic acid crosslinked with alginate hydrogel: A versatile and biocompatible bioink platform for tissue engineering

Truc Nguyen Thanh [a], Navaporn Laowattanatham [b], Juthamas Ratanavaraporn [c,d], Amornpun Sereemaspun [e], Supansa Yodmuang [d,f,g,*]

[a] Medical Sciences Program, Faculty of Medicine, Chulalongkorn University, Bangkok 10330, Thailand
[b] Winner Prototype, Lat Phrao 122, Phlabphla, Wang Thonglang, Bangkok 10312, Thailand
[c] Biomedical Engineering Program, Faculty of Engineering, Chulalongkorn University, Bangkok 10330, Thailand
[d] Biomaterial Engineering for Medical and Health Research Unit, Chulalongkorn University, Bangkok 10330, Thailand
[e] Department of Anatomy, Faculty of Medicine, Chulalongkorn University, Bangkok 10330, Thailand
[f] Research Affairs, Faculty of Medicine, Chulalongkorn University, Bangkok 10330, Thailand
[g] Excellence Center for Advanced Therapy Medicinal Products, King Chulalongkorn Memorial Hospital, Bangkok 10330, Thailand

ARTICLE INFO

Keywords:
Hyaluronic acid
Alginate
3D bioprinting
Bioink
Cartilage tissue

ABSTRACT

Three-dimensional bioprinting holds promise in the anatomical fabrication of lost tissues and organs. Cell-laden hydrogels have been widely used as bioinks, extruded through a nozzle of 3D bioprinter to form the desired shape layer-by-layer. However, the major challenge in 3D bioprinting is finding functional biomaterials to develop bioinks, besides animal-based biomaterials, such as gelatin and collagen. The amine-hyaluronic acid (HA-NH_2) was covalently crosslinked with the aldehyde-alginate (Alg-CHO). Once HA-NH_2 and Alg-CHO solutions combine, by varying volume ratios, gelation is initiated through a Schiff's base reaction. The goal of this study was to investigate how volume ratios of HA-NH_2 and Alg-CHO had impacts on the printability and biodegradability of the HA-Alg hydrogel and its potential use in the chondrogenic differentiation of mesenchymal stem cells (hMSCs). The HA-Alg hydrogel made from equal volumes of HA-NH_2 and Alg-CHO exhibited shear-thinning behaviours, which are essential features of a printable bioink. Moreover, we demonstrated cartilage tissue formation by encapsulating hMSCs in the HA-Alg hydrogel for 4 weeks. To demonstrate a proof-of-concept in creating an interpenetrating polymer network (IPN), the incorporation of silk fibroin into the HA-Alg hydrogel network was tested. This finding allowed the HA-Alg hydrogel to serve as a platform for development of other bioinks, without adverse effects on mechanical properties and shear-thinning behaviours. The results suggest that the HA-Alg hydrogel can be used as a printable biomaterial for the extrusion-based 3D bioprinter. The HA-Alg hydrogel promoted cartilage tissue development and potentially supported other tissue formation due to its tailorable mechanical and degradable properties.

1. Introduction

Development of three-dimensional (3D) bioprinting technology has increased significantly to alleviate the organ shortage crisis. In conjunction with tissue engineering, the 3D bioprinting offers a potential application in the fabrication of anatomically shaped implants for tissue reconstruction, such as bone, cartilage and skin [1–4]. The extrusion-based 3D bioprinting involves the dispensing of bioink using the nozzle extruder incorporated with an x, y, z motion system. One of the most challenging issues facing extrusion-based platforms is to develop bioinks following two key additive manufacturing requisites, which are printability and biocompatibility [5,6]. To meet these requirements, selecting the appropriate functional biomaterials is of utmost importance. Biomaterial-based hydrogels, both natural and synthetic, have been attractive candidates for bioinks and their excellent hydrophilicity has been a determining factor. Advantages of hydrogels include their fine control over viscosity, crosslinking, and surface tension of bioink, as well as their provision of a microenvironment for cell growth and tissue formation [7–9].

Among the bioink materials used for 3D tissue printing, a bacterial

* Corresponding author at: Research Affairs, Anunda Mahidol Building, Faculty of Medicine, Chulalongkorn University, 1873 Rama 4 Rd, Pathumwan, Bangkok 10330 Thailand.
E-mail address: supansa.y@chula.ac.th (S. Yodmuang).

https://doi.org/10.1016/j.eurpolymj.2022.111027
Received 18 November 2021; Received in revised form 3 January 2022; Accepted 19 January 2022
Available online 24 January 2022

hyaluronic acid (HA) hydrogel is a promising candidate [10,11]. HA, composed of repeat units of β-1,4-D-glucuronic acid and β-1,3-N-acetyl-D glucosamine, is a polymeric glycosaminoglycan (GAG) originally found in the extracellular matrix (ECM) of articular cartilage [12,13]. For decades, HA has been widely investigated in biomedical research, especially in cartilage regeneration [10,13–15]. The presence of HA plays a critical role in maintaining cartilage homeostasis, promotes chondrogenic phenotypes, and stimulates type II collagen production [16]. Despite the outstanding biocompatibility and hydrophilicity of HA, its application as bioink in 3D bioprinting is very limited because of its low viscosity, difficult gelation process, and low mechanical properties. Many attempts have been made to address these challenges, including combining HA with chitosan [17], crosslinking with collagen and poly(ethylene glycol) ether tetrasuccinimidyl glutarate [18]. To date, the practical applications of HA in 3D bioprinting have not been clearly identified.

Taken together, this has led our research group to develop new bacterial HA-based bioinks. The manufacturing strategy was developed the composite hydrogel by combining the biocompatible advantages of HA with a mechanically stable biopolymer, alginate (Alg). Derived from brown algae, Alg contains β-D-mannuronate (M blocks) and α-L-gulur-onate (G blocks) subunits bonded with 1, 4 linkages. Mechanical properties of Alg are usually modulated by ionic interactions between G blocks and Ca^{2+} or other divalent cations to form 3D "egg box" structures [19]. Hence, the objectives of this study were to develop a printable HA-Alg hydrogel and investigate its potential use in the chondrogenic differentiation of hMSCs.

We hypothesized that the HA-Alg hydrogel exhibits shear-thinning behaviours to allow 3D bioprintability without cytotoxicity. To test this hypothesis, bacterial HA and Alg were modified to amine-hyaluronic acid (HA-NH_2) and aldehyde-alginate (Alg-CHO), respectively. HA-NH_2 and Alg-CHO were covalently crosslinked and formed the HA-Alg hydrogel via imine bonds between amino and aldehyde groups, known as Schiff's base reaction [20]. By varying the volume ratios of HA-NH_2 and Alg-CHO, the hydrogel exhibited a wide range of printability and degradability. The functional groups of HA-Alg were characterized by magnetic nuclear resonance (NMR) and Fourier transformed infrared spectroscopy (FTIR). The viscosity and shear-thinning behaviour of the hydrogel were investigated by rheological analysis. Printability was tested using an extrusion-based 3D bioprinter. Hydrogel degradation was investigated over 60 days in physiological PBS solution. Human mesenchymal stem cells (hMSCs) were encapsulated into HA-Alg hydrogels and tested for cytotoxicity and cartilage tissue formation.

The potential application of HA-Alg hydrogel as an interpenetrating polymer network (IPN) platform to entrap other biopolymers was investigated by incorporating silk fibroin (SF), a macromolecular structure containing amino groups. HA-Alg hydrogel could optimize properties by varying the volume ratios of HA-NH_2 and Alg-CHO. The versatility of HA-Alg hydrogel, including its uses in bioink and IPN platform, suggests the creation of bioprinted tissue constructs with desirable mechanical properties and a tuneable biodegradation time.

2. Materials and methods

2.1. Materials

Hyaluronic acid sodium salt (molecular weight 1.6 × 10^6 Da) (53747), sodium alginate (W201502), lithium bromide (LiBr) (213225), ethylenediamine (753084), 1-hydroxybenzotriazole hydrate (HOBt) (54802), 1-ethyl-3-(3-dimethylaminopropyl) carbodiimide hydrochloride (EDC) (03450), sodium periodate ($NaIO_4$) (S1878), ethylene glycol (324558), sodium chloride (NaCl) (S9888), and dimethyl sulfoxide (DMSO) (D48418) were purchased from Sigma-Aldrich (St, Louise, MO, USA). HyClone Minimal Essential Medium (αMEM) used for cell culture was purchased from Cytiva (Logan, Utah, USA). High-glucose DMEM (D7777), insulin-transferrin-selenium liquid medium supplement (I3146), L-Proline (147853), dexamethasone (D4902), and ascorbic acid (A4544) were purchased from Sigma-Aldrich (St. Louis, MO, USA). Gibco™ HEPES (15630080), Gibco™ antibiotic–antimycotic (15240062), Gibco™ fetal bovine serum (FBS) (A4766801), human TGF-β3 recombinant protein (RP8600) were purchased from Thermo-Fisher Scientific (Waltham, MA, USA). TrypLE™ Express Enzyme (12604021), Invitrogen™ LIVE/DEAD® viability/cytotoxicity kit (L3224), PrestoBlue™ (P50200), and Quant-iT™ Picogreen™ dsDNA Assay were purchased from ThermoFisher Scientific (Waltham, MA, USA).

2.2. Synthesis of HA-NH_2

HA was dissolved in deionized (DI) water to make a concentration of 5 mg/mL. A 30-molar excess of ethylenediamine was added into the HA solution. The pH of the solution was adjusted to 6.5 by HCl, resulting in the reaction mixture. Next, EDC (0.8 g) and HOBt (0.7 g) were dissolved in 10 mL of DMSO in water (1: 1 v/v) and added dropwise to the reaction mixture [21]. The HA reaction mixture was stirred for 24 h at room temperature and dialyzed (molecular weight cut-off 14000 Da, Sigma-Aldrich, MO, USA) against DI water for 3 days. The solution after dialysis was subjected to salting out by addition of NaCl to final concentration of 5% w/v. The white HA-NH_2 precipitation was collected in 70% ethanol, redissolved in water, and then dialyzed for 3 days. The final product was freeze-dried and stored at 4 °C.

2.3. Synthesis of Alg-CHO

Alg was dissolved in DI water to obtain a concentration of 2% w/v. The 5 mL of 0.5 M $NaIO_4$ was added to Alg solution and stirred for 2 h at room temperature in the dark. Ethylene glycol (1 mL) was used to quench the excess $NaIO_4$. The resulting solution was stirred for 2 h and then dialyzed against DI water for 3 days. The solution in dialysis bag was freeze-dried, and stored at 4 °C.

2.4. Preparation of SF

The 4 g of degummed silk was dissolved in 16 mL of 9.3 M LiBr solution at 60 °C for 4 h. The resulting solution was collected and dialyzed against DI water for 3 days. Subsequently, the dialyzed SF solution was centrifuged at 9000 rpm, 4 °C for 20 min twice to separate SF solution from debris [22]. The SF concentration was determined by weighing the remaining solid after drying.

2.5. Preparation of HA-Alg hydrogel

The dry products of HA-NH_2 and Alg-CHO were dissolved separately in 1xPBS to reach a concentration of 30 mg/mL and 20 mg/mL, respectively. The HA-Alg hydrogels were fabricated by thoroughly mixing HA-NH_2 and Alg-CHO solutions at various volume ratios of 2:8, 3:7, 4:6, 5:5, 6:4, 7:3, and 8:2 at room temperature (Table 1).

Table 1
HA-Alg hydrogels at different volume ratios of HA-NH_2 and Alg-CHO. O: Form gel, X: Do not form gel.

Volume ratio	HA-NH_2 (μL)	Alg-CHO (μL)	Gelation
2:8	40	160	X
3:7	60	140	X
4:6	80	120	X
5:5	100	100	O
6:4	120	80	O
7:3	140	60	O
8:2	160	40	X

2.6. Preparation of HA-Alg-SF hydrogel

HA-NH_2 was dissolved in 1xPBS and added to SF solution to make a final concentration of 30 mg/mL HA-NH_2 and 2 mg/mL SF, resulting in HA-NH_2/SF mixture. Then, the 20 mg/mL of Alg-CHO was added to the HA-NH_2/SF mixture based on a volume ratio of HA-NH_2/SF: Alg-CHO (5:5). The concentration of SF (2 mg/mL) loaded in the HA-Alg was determined from our previous research [23].

2.7. Characterization of HA-Alg and HA-Alg-SF hydrogel

2.7.1. NMR analysis

The pure HA, Alg, freeze-dried HA-NH_2, and freeze-dried Alg-CHO were dissolved in deuterium oxide (D_2O) and transferred to 5 mm NMR sample tubes. The NMR spectra were recorded by Bruker AVANCE III 500 MHz spectrometer (Billerica, MA, USA). One-dimensional ^1H and ^{13}C resonances were obtained and analysed using Mnova (Mestrelab, ver.14.1).

2.7.2. FTIR analysis

The freeze-dried samples were ground with KBr powder. FTIR spectra were obtained in a wavenumber range from 4000 cm^{-1} to 500 cm^{-1}. The spectrum was averaged over 64 scans with 4.0 cm^{-1} resolutions (Perkin Elmer, Spectrum One, USA). The spectra were documented and analysed using Origin (Origin Lab, ver.2021).

2.7.3. Swelling and degradation analysis

The initial wet weight (W_0) of hydrogels (n = 3) was recorded. Then hydrogels were submerged in 1xPBS solution (pH 7.4) at 37 °C for 60 days. Hydrogels were removed from PBS solution, with wet weight (W_t) recorded at different timepoints to calculate percentage of weight differences, W_d (%), as described in the equation below.

$$W_d\ (\%) = (W_t - W_0)/W_0 \times 100$$

The positive and negative values were expressed in swelling (%) and degradation (%), respectively.

2.7.4. Printability of HA-Alg (5:5) and HA-Alg-SF hydrogel

The Alg-CHO was mixed with an equal volume of HA-NH_2 or HA-NH_2/SF, transferred into a 1-ml syringe and printed through an 18G needle (outer diameter: 1.27 mm, inner diameter: 0.84 mm) using a custom-made 3D printer equipped with a screw-driven extruder (Enterprise 2.0) (Fig. 6A). The printed patterns were designed by Blender software (Blender, ver.9.3 LTS), and the G-code files were generated using a slicing software (Simplify3D ver.4.0). HA-Alg or HA-Alg-SF hydrogels were printed into 5 layers of grid patterns (total dimension was 20 mm × 20 mm × 5 mm). The printing condition was maintained at 37 °C with a speed of 60 mm/min.

To investigate the cell-loading capacity of the hydrogel for bioprinting, the Alg-CHO was mixed with FluoSpheres™ Polystyrene Microsphere (F8834, Invitrogen, MA, USA), combined with an equal volume of HA-NH_2, transferred into a 1-ml syringe, and printed through an 18G needle followed the previously described procedure. The distribution of the microspheres in the HA-Alg hydrogel was visualized under a confocal microscope (Zeiss LSM 800, Germany).

Cell viability assessment in 3D-printed constructs was conducted by encapsulating hMSCs in the HA-Alg or HA-Alg-SF hydrogels. hMSCs were mixed with Alg-CHO, combined with an equal volume of HA-NH_2 solution or HA-NH_2/SF mixture, and transferred into a 1-ml syringe (10^6 cells/mL). The cell/hydrogel was printed through 18G needle into 2 layers of grid patterns (total dimension was 15 mm × 15 mm × 0.2 mm). Cell viability was observed under fluorescence microscope (Nikon Eclipse Ti, USA) 1 day post-printing.

2.7.5. Mechanical assessment of hydrogels

Mechanical properties of hydrogels (n = 3) were measured by a Hounsfield electronic universal testing machine (Hounsfield HT, USA) at room temperature. The hydrogels of 13 mm in diameter and 10 mm in thickness were placed into the testing machine with a constant velocity of 10 mm/min in compressive mode. All hydrogel samples were compressed to 50% of the height of their original cylindrical shape.

2.7.6. Rheological analysis of hydrogels

Rheological measurements of hydrogels were performed with a rheometer (HAAKE MARS III, ThermoScientific, USA) equipped with parallel plates set in oscillatory mode at room temperature. Strain sweep experiment was conducted over a range of 0.1–100%, at 1 Hz to determine the linear viscoelasticity region (LVER) of the hydrogels. Then, the dependence/independence of elastic modulus (G′) and viscous modulus (G″) over a range of oscillation frequencies (0.01–100 Hz) was acquired at the defined strain rate. Time sweep experiment was performed to determine the gelation time at 1 Hz, for 30 min and at room temperature. The viscosity of hydrogels over a shear rate (0.001–1000 s^{-1}) was recorded.

2.8. Investigation of cartilage tissue formation in hydrogel

2.8.1. Sample sterilization

Chemical modification of HA and Alg was conducted in a biosafety cabinet. All chemicals and reagents were filtered before use. The lyophilized HA-NH_2 and Alg-CHO were sterilized under UV light for 20 min in a biosafety cabinet prior to in vitro experiments.

2.8.2. Cell culture and encapsulation in hydrogel

hMSCs (Lonza, Walkersville, MD) were maintained in hMSC medium (αMEM supplemented with 5% (v/v) FBS, 1% (v/v) GlutaMAX, 1% (v/v) HEPES buffer, 1 ng/mL of fibroblast growth factor-basic (bFGF) (Invitrogen), and 1% (v/v) antibiotic–antimycotic solution) at 37 °C and 5% CO_2. The medium was changed every 3 days. Subculturing was performed using TrypLE™ Express when cells reached 80% confluency. For cell encapsulation, the Alg-CHO solution was mixed with hMSCs first and then added with an equal volume of HA-NH_2 solution or HA-NH_2/SF mixture (1×10^6 cells/mL). The 50 mL of HA-Alg or HA-Alg-SF mixture was transferred into 6 mm × 8 mm cloning rings (Pyrex, Sigma Aldrich) and incubated at 37 °C, 5% CO_2 for 2 h. Then, cell/hydrogel constructs were pushed out from cloning rings and further cultured in chondrogenic medium.

2.8.3. Live/dead assay

According to ISO standard 10993–5:2009, hydrogels were directly assessed using cytotoxicity by LIVE/DEAD® Kit. The constructs (n = 3) were incubated in Calcein AM/EthD-1 for 30 min in the dark. The hydrogel constructs were visualized using an inverted fluorescence microscope (Nikon Eclipse Ti, USA) to determine living (green) and dead (red) cells on day 1, 3 and 7 post-encapsulation. This will ensure cell viability in hydrogels at the early stage of encapsulation.

2.8.4. PrestoBlue™ assay

The constructs (n = 3) on day 1, 3 and 7 post-encapsulation were incubated with 1x PrestoBlue™, at 37 °C, 5% CO_2 for 3 h. Then, the incubated medium was taken out and transferred to a 96-well plate. The fluorescence was measured at λ_{ex} 560 nm and λ_{em} 590 nm using a microplate reader (Varioskan Lux, Thermo Scientific, USA). Fibrin hydrogel was used as control due to its compatibility for cell encapsulation [24]. Blank wells were HA-Alg (5:5), HA-Alg-SF, and fibrin hydrogels without cell encapsulation.

2.8.5. Quant-iT™ Picogreen™ dsDNA Assay

The constructs (n = 3) were removed from culture medium, minced, and digested in 1 mg/mL proteinase K (P2308, Sigma-Aldrich, MO, USA) containing 20 μL papain solution (P4762, Sigma-Aldrich, MO, USA). DNA content was measured using Quant-iT™ Picogreen™ dsDNA Assay

Kit. Samples were measured at λ_{ex} 480 nm and λ_{em} 530 nm using a microplate reader (Varioskan Lux, Thermo Scientific, USA).

2.8.6. Chondrogenic differentiation

The hMSCs/hydrogel constructs ($1x10^6$ cells/mL) were cultured in chondrogenic medium (high-glucose DMEM supplemented with 1% (v/v) insulin–transferrin–selenium, 1% (v/v) HEPES buffer, 0.1% (v/v) L-proline, 0.1% (v/v) ascorbic acid, 0.4 μg/mL of dexamethasone, 5 ng/mL of TGF-β3, and 1% (v/v) antibiotic–antimycotic) for 4 weeks, with medium changes every 3 days.

2.9. Immunofluorescent staining

After 2 weeks and 4 weeks, the constructs were fixed in 4% formaldehyde and embedded in cryogel (FCS 22 Clear, Leica). The constructs were sectioned with 5 μm thick. The sections were pre-treated with proteinase K for antigen retrieval, rinsed with PBS, incubated with blocking serum, and incubated with 1: 200 rabbit polyclonal to type II collagen antibody (ab34712, Abcam, UK) for 1 h. After that, the sections were washed and incubated with anti-rabbit secondary antibody conjugated with Texas Red (ab7088, Abcam, UK) for 1 h at room temperature in the dark. Negative control samples were sections without primary antibody incubation. All samples were mounted with a fluoroshield mounting medium with DAPI (ab104139, Abcam, UK). The sections were visualized under an inverted fluorescence microscope (Nikon Eclipse Ti, USA).

2.10. Statistical analysis

Statistical analysis was performed using Stata (StataCorp, ver.17). Data were expressed as mean ± standard deviation (SD) of n = 3 unless otherwise specified. The differences in mechanical testing, cell proliferation in PrestoBlue™ and Quant-iT™ Picogreen™ dsDNA Assay were evaluated using *t*-test and one-way ANOVA, followed by Tukey's post-test with $\alpha = 0.05$ to consider statistical significance.

3. Results

3.1. NMR analysis of HA-NH_2 and Alg-CHO

^{1}H NMR was performed to characterize the native HA and confirm the modification of HA with amino groups (—NH_2). In the spectrum of HA, the signals from 3.87 to 3.43 ppm were assigned to the protons on the sugar rings (Fig. 1A) [25,26]. The carboxylate groups of HA were activated and conjugated with the primary amines from ethylenediamine using EDC/HOBt. The methyl (—CH_3) protons of the N-acetyl group of HA and HA-NH_2 showed a signal at 2.06 ppm and 2.03 ppm (Fig. 1, label a). In the spectrum of HA-NH_2, the presence of conjugated ethylenediamine was confirmed by the proton signals at 3.20 ppm (Fig. 1B, label b) and 2.93 ppm (Fig. 1B, label c) [27]. HA-NH_2 also exhibited the new proton signals at 3.94 and 3.37 ppm (Fig. 1B), indicating the chemical shift in protons in the sugar rings after conjugation with primary amines.

Alg and Alg-CHO were characterized by ^{1}H and ^{13}C NMR to confirm the products of oxidation. Alg was reacted with $NaIO_4$ resulting in the cleavage of the carbon bond between C-2 and C-3, leading to the formation of two aldehyde groups on its polymer chains, as indicated by Alg-CHO (Fig. 2A). The ^{1}H NMR spectra of Alg and Alg-CHO exhibited the signals at 5.06, 4.66, and 4.48 ppm, corresponding to the protons at the position of G1, M1, 5 and G5 on the Alg backbone (Fig. 2B) [28]. The peaks at 9.3–9.7 ppm representing aldehyde groups were not detected on the ^{1}H NMR spectrum of Alg-CHO. Instead, the peaks at 5.74 and 5.55 ppm, which were reported as the signals of hemiacetal after oxidation of alginate with $NaIO_4$ [29], were detected (Fig. 2B). The highly unstable aldehyde groups on Alg-CHO react with the hydroxyl groups (—OH) on the adjacent sugar rings and form hemiacetal, which is reversible in aqueous environment (Fig. 2A).

For ^{13}C NMR spectra, both Alg and Alg-CHO showed the signals corresponding to G blocks (G1, G2, G3, G4 and G5) and M blocks (M1, M4 and M5) on their sugar rings (Fig. 2C) [30]. The ^{13}C NMR spectrum of Alg-CHO had the new signals at 95.09 ppm and 92.73 ppm which were assigned to hemiacetalic carbons. Although the signal of aldehyde groups on Alg-CHO were not present in the NMR spectra, the signals of hemiacetalic protons demonstrated successful modification of Alg to Alg-CHO.

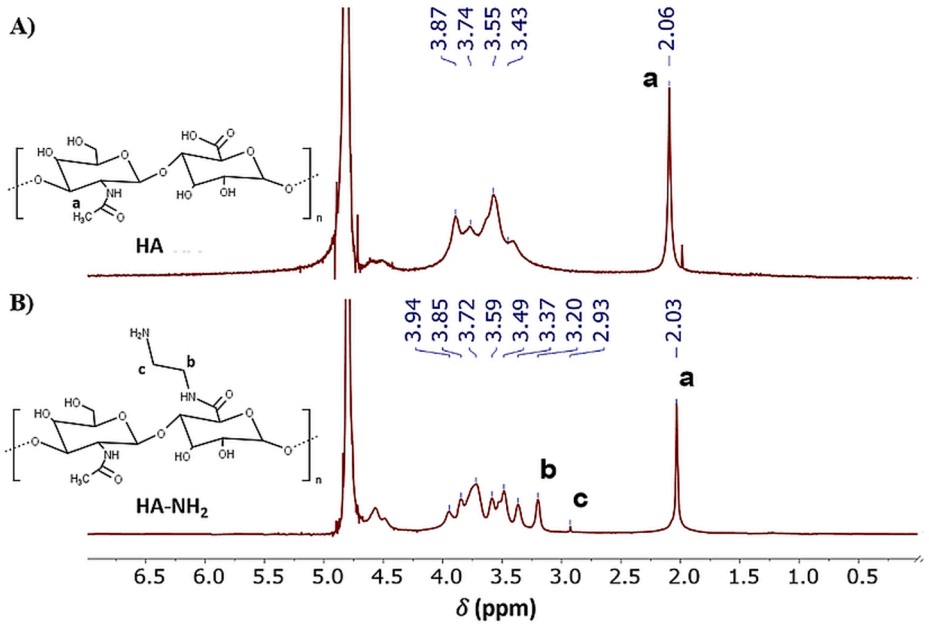

Fig. 1. ^{1}H NMR spectra of (A) unmodified HA, and (B) modified HA-NH_2.

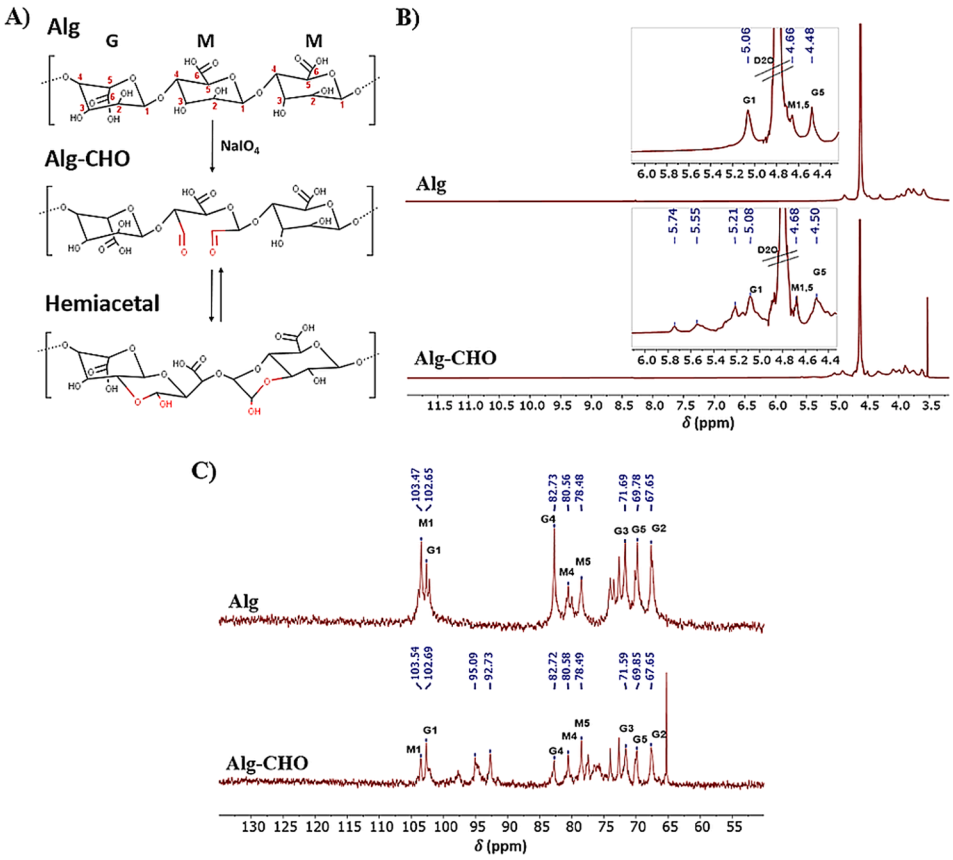

Fig. 2. (A) Oxidation of Alg by $NaIO_4$ to form Alg-CHO and the formation of intramolecular hemiacetal as an intermediate product, (B) The ^{1}H NMR spectra of Alg and modified Alg-CHO, and (C) The ^{13}C NMR spectra of Alg and modified Alg-CHO.

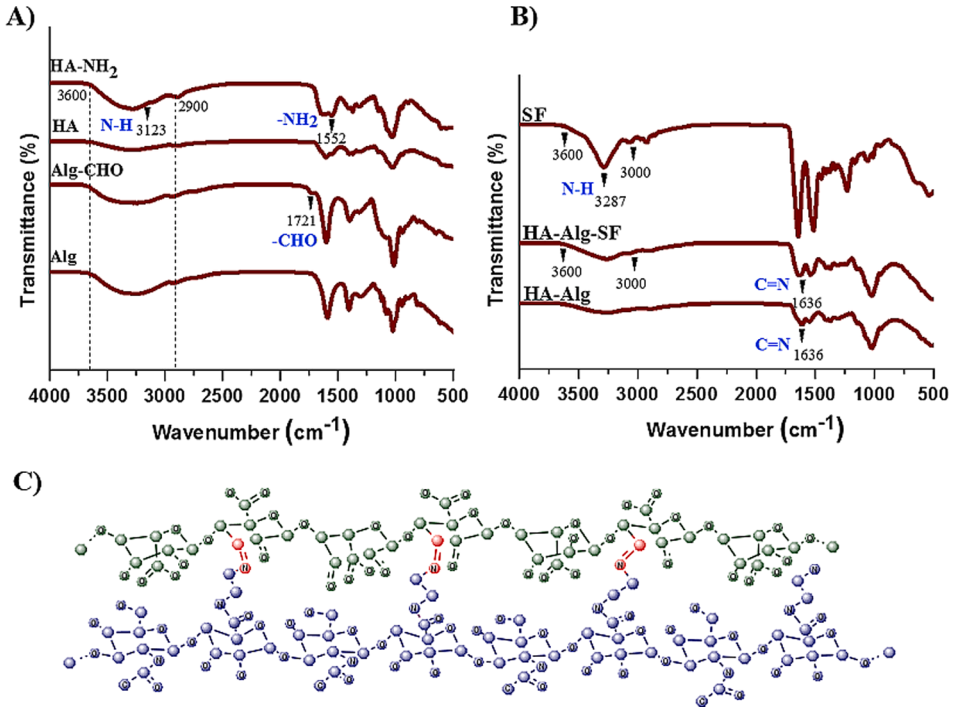

Fig. 3. FTIR analysis of (A) $HA\text{-}NH_2$, HA, Alg-CHO and Alg, (B) extracted SF, HA-Alg-SF hydrogels and HA-Alg (5:5) hydrogel, and (C) Schiff's base crosslinked HA-Alg hydrogel (green = Alg-CHO, purple = $HA\text{-}NH_2$). (For interpretation of the references to colour in this figure legend, the reader is referred to the web version of this article.)

3.2. FTIR analysis of HA-NH_2, Alg-CHO and HA-Alg hydrogels

FTIR spectra of HA and Alg were determined before and after modification to confirm the addition of amino groups (—NH_2) and aldehyde groups (—CHO) on HA and Alg, respectively (Fig. 3A). FTIR spectrum of HA showed the stretching O—H of the hydroxyl groups at 3600–2900 cm^{-1}. In the spectrum of HA-NH_2, a new peak at 3123 cm^{-1} was observed, which indicated the presence of N—H stretching in amine salt after chemical modification. The primary amines (—NH_2) in HA-NH_2 were confirmed by the peak at 1552 cm^{-1}. For Alg-CHO modification, the peak at 1721 cm^{-1} of aldehyde groups (—CHO) was observed [31]. Gelation of HA-Alg hydrogel occurred as a result of imine bond (C═N) formation via Schiff's base reaction between —CHO and —NH_2 groups (Fig. 3C), as demonstrated by the peak at 1636 cm^{-1} (Fig. 3B) [32].

When SF was incorporated into the HA- Alg matrix, the secondary amine (N—H stretching) of HA-Alg-SF hydrogel was clearly observed at higher intensity than that of HA-Alg hydrogel, as demonstrated at 3600–3000 cm^{-1} region and the peak at 3287 cm^{-1} [33]. SF contains a very low quantity of primary amines (—NH_2) in Lysine (<0.5 mol%) [34], which unlikely react with aldehyde groups (—CHO) on modified Alg-CHO. Depletion of aldehyde groups at peak 1721 cm^{-1} in both HA-Alg and HA-Alg-SF hydrogels resulted from the reaction between Alg-CHO and HA-NH_2. The crosslink of HA-Alg-SF hydrogel is mainly based on Schiff's base reaction between Alg-CHO and HA-NH_2.

3.3. Gelation of HA-Alg at different volume ratios

The HA-Alg hydrogel was formed by combining HA-NH_2 and Alg-CHO solutions at different volume ratios. HA-NH_2 and Alg-CHO solutions at volume ratios of 5:5, 6:4, and 7:3 were able to form hydrogels (Table 1 and Fig. 4). Different ratios of HA-NH_2 and Alg-CHO influenced hydrogel formation and injectability through needles (Fig. 4). Among the hydrogel groups, gelation took longer when the ratio of HA-NH_2 solution increased. For the ratio of 5:5, gelation occurred within 2 min and showed more rigidity compared to other ratios. Therefore, the volume ratio of HA-NH_2 and Alg-CHO at 5:5 was chosen for SF entrapment in HA-Alg network, resulting in HA-SF-Alg hydrogel (Fig. 4)

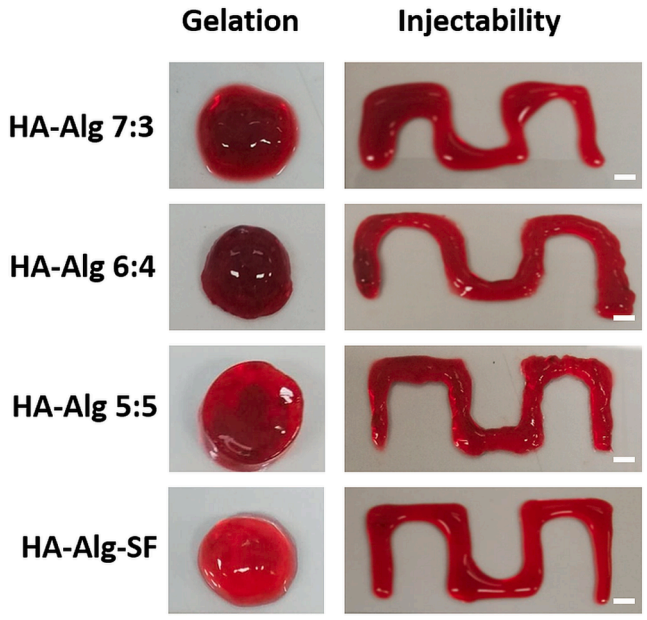

Fig. 4. Morphology and injectability of HA-Alg hydrogels at different volume ratios of HA-NH_2 and Alg-CHO. The HA-Alg-SF hydrogel made from HA-NH_2 and Alg-CHO at volume ratio of 5:5 (scale bars: 1 mm).

3.4. Swelling and degradation behaviours of hydrogels

The wet weights of hydrogels were recorded at each timepoint and compared to the wet weight in day 0 (Fig. 5, Supplementary Table S1). Compared to other formulations, the HA-Alg (7:3) hydrogel exhibited a significantly increased weight (swelling) from day 5 (4.8 ± 2.5%) to day 10 (8.6 ± 2.1%), and the fastest weight loss to 95.4 ± 8.0% in 40 days. The HA-Alg (6:4) hydrogel slightly increased wet weight up to day 10 (3.8 ± 2.4%) and decreased to 89.4 ± 5.3% on 40 days. Interestingly, the swelling and degradation profiles of HA-Alg (5:5) hydrogel remained constant for up to 35 days, before the hydrogel slowly degraded to 38.3 ± 14.9% on day 60.

When increasing the volume ratio of HA-NH_2 to Alg-CHO in the hydrogel, the HA-NH_2 can absorb more water due to the interaction between hydroxyl groups on its backbone and water molecules. The molecular structure of HA-NH_2 stretched out, water content in the hydrogels increased, and a high swelling pressure developed [35]. Generally, swelling pressure in hydrogel counteracts with the tensile strengths of the hydrogel network. It is possible that an increase in swelling pressure reduces the rigidity of the hydrogel network, which induces the degradation of hydrogel [36]. Hydrogels will eventually be replaced by a new extracellular matrix from cells. We demonstrated modulation of the volume ratio of HA-NH_2 and Alg-CHO could control degradation of the HA-Alg hydrogel, which could broaden the applications of the HA-Alg hydrogel to the reconstruction of many types of tissue.

For the HA-Alg-SF hydrogel, the wet weight increased until day 20 (8.7 ± 2.4%). After that, this hydrogel started to degrade from day 25 and remained only 17.2 ± 0.8 % on day 60. The addition of SF resulted in faster degradation of the HA-Alg-SF hydrogel compared to the HA-Alg (5:5) hydrogel. Based on swelling and slow degradation profiles, the HA-Alg (5:5) hydrogels with and without SF were chosen to assess printability, mechanical properties and cartilage tissue formation.

3.5. Printability of HA-Alg (5:5) and HA-Alg-SF hydrogels

The HA-Alg (5:5) and HA-Alg-SF hydrogels served as bioink for our custom-made 3D printer (Fig. 6A). The HA-Alg (5:5) and HA-Alg-SF hydrogels were able to print, as demonstrated by the defined strands and structural integrity after printing (Fig. 6B). The fluorescent microspheres encapsulated in the hydrogel displayed homogenous distribution in line patterns (Fig. 6C). Moreover, hMSC-loaded hydrogels with and without SF which were printed in two layers of grid patterns showed excellent biocompatibility and hMSCs did not affect by shear stress

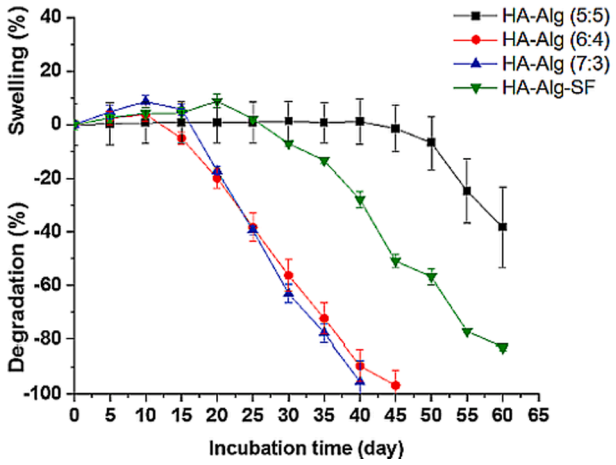

Fig. 5. Swelling and degradation profiles of HA-Alg hydrogels at different volume ratios, and HA-Alg-SF hydrogels. The data were displayed as mean ± SD (n = 3).

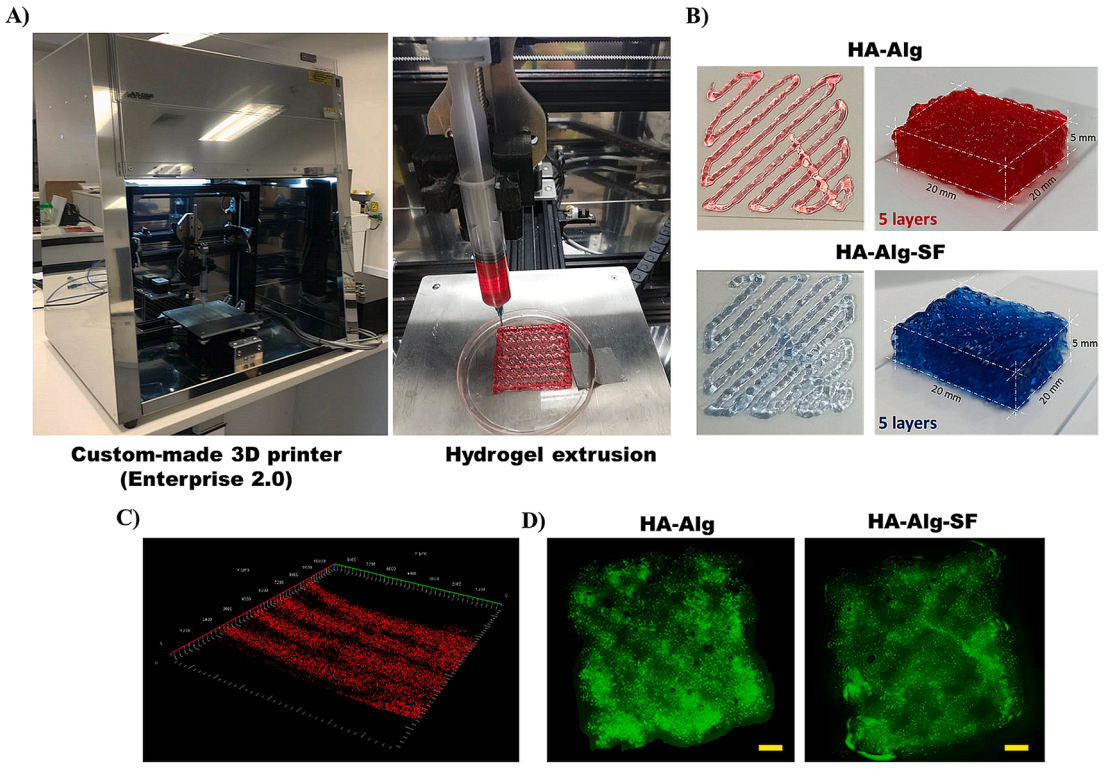

Fig. 6. Printability of hydrogels. (A) Custom-made printer (Enterprise 2.0), (B) The 3D-printed HA-Alg (5:5) and HA-Alg-SF hydrogels (bioinks), (C) The distribution of fluorescent microspheres in the 3D-printed HA-Alg hydrogel (bioink), and (D) Cell viability of human mesenchymal stem cells (hMSCs) in the hydrogels, 1 day post printing (scale bars: 2 mm).

during extrusion, as demonstrated by green live cells (green dots) (Fig. 6D).

Besides printability, cell viability is major concern for the success of bioprinting, where cells will experience an instant shear stress while passing through a nozzle. The levels of shear stress are well-controlled by the viscosity of hydrogels and the printing parameters [37]. The size of the needle gauge is a key factor that affects cell viability post-printing. A smaller needle diameter develops higher shear stress, resulting from a greater force needed to eject the gel [38]. Meanwhile, an appropriate printing speed was also investigated to ensure the pattern printability [39]. Here, the printing parameters, including room temperature, 18G needle, and 60 mm/min speed of the custom-made 3D bioprinter, facilitated the deposition of HA-Alg (5:5) and HA-Alg-SF hydrogels, and did not affect hMSC viability during the printing process.

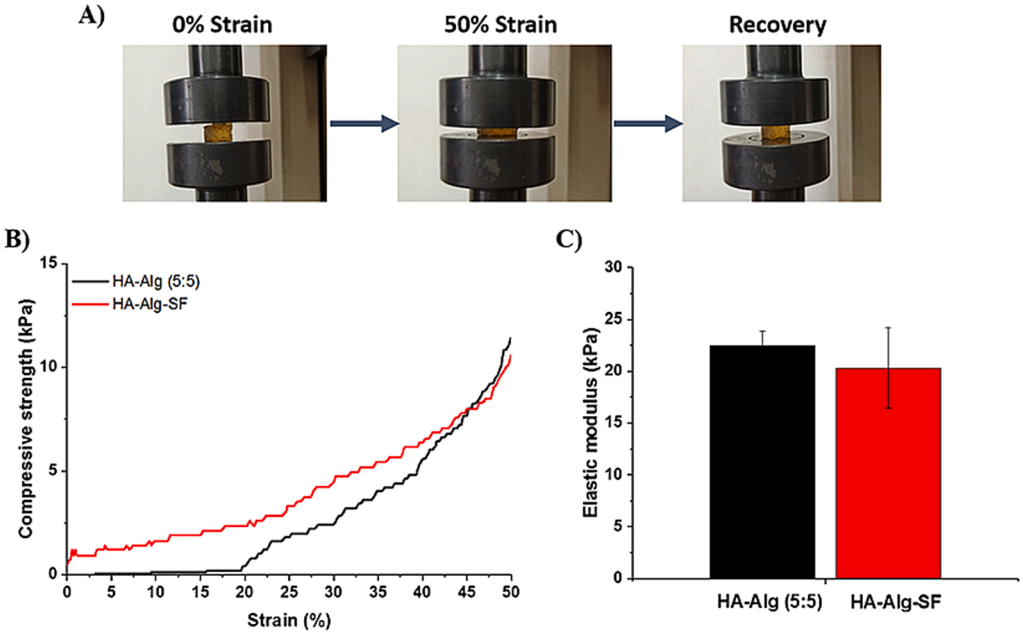

Fig. 7. Compressive strength of hydrogels. (A) Recovery ability of the HA-Alg (5:5) hydrogel after compression, (B) Compressive stress–strain curve of HA-Alg (5:5) and HA-Alg-SF hydrogels, and (C) The elastic modulus of HA-Alg (5:5) and HA-Alg-SF hydrogels.

When combined with 3D printing technology and medical imaging, the HA-Alg (5:5) hydrogel could be printed into ear-shape structure for reconstructive surgery (Supplementary Fig. S1). HA-Alg (5:5) and HA-Alg-SF hydrogels have great potential as bioinks for 3D bioprinting and the differentiation of chondrocytes.

3.6. Mechanical assessment of hydrogels

Under compressive loading, both HA-Alg (5:5) and HA-Alg-SF hydrogels could withstand the load at 50% strain and recovered to their original shapes (Fig. 7A). The compressive strength of HA-Alg (5:5) and HA-Alg-SF hydrogels were 11.44 ± 1.80 kPa and 10.61 ± 0.36 kPa, respectively, at the strain of 50% (Fig. 7B, Supplementary Table S2). The incorporation of SF did not show a significant difference in elastic modulus between the two hydrogels (HA-Alg hydrogel = 22.5 ± 1.36 kPa vs. HA-Alg-SF hydrogel = 20.31 ± 3.90 kPa, $p > 0.05$) (Fig. 7C).

3.7. Rheological analysis of hydrogels

Initially, a strain sweep test was used to determine the linear viscoelasticity region of the hydrogel, which indicated the range of strain amplitudes that do not destroy the hydrogel structure. Here, the strain sweep from 0.1% to 100% was conducted at 1 Hz on both hydrogels. The storage (G′) and loss (G″) moduli were found to be beyond 100% for both HA-Alg (5:5) and HA-Alg-SF hydrogels (Fig. 8A). This study suggested that the HA-Alg (5:5) and HA-Alg-SF hydrogels exhibited high stretchability and large deformation. The frequency sweeps from 0.01 Hz to 100 Hz were carried out at 1% strain, corresponding with the determined LVE strain amplitude (Fig. 8B). The crossover points between G′ and G″ for HA-Alg (5:5) and HA-Alg-SF were 78 Hz (black and red lines) and 61 Hz (blue and green lines), respectively (Fig. 8B). Below these points, the elastic behaviour dominated the properties of the hydrogels (G′ > G″). On the other hand, exceeding the crossover point, both hydrogels showed a more fluid-like behaviour at a high frequency, suggesting that the high frequency interrupted the hydrogel structure. Both hydrogels, G′ and G″, showed frequency dependence throughout the range test, from 1 Hz to 100 Hz. The time sweep of HA-Alg (5:5) and HA-Alg-SF hydrogels was expected to provide information on gelation time. In principle, the gelation of hydrogel has been observed by the crossover time between storage (G′) and loss (G″) moduli. Before the gelation, G″ is greater than G′, which shows the liquid behaviour. When the gelation occurs, G′ is equal to G″ and ultimately exceeds G″ value according to time. Although the gelation points of HA-Alg (5:5) and HA-Alg-SF hydrogels were not detected, G′ was greater than G″ in both hydrogels, indicating the elastic behaviour of crosslinked hydrogels (Fig. 8C). The absence of a gelation point could be explained by the quick reaction of HA-NH_2 and Alg-CHO before loading into the plate geometry of rheometer.

In both HA-Alg (5:5) and HA-Alg-SF hydrogels, the viscosity decreased when shear rate increased (Fig. 8D). The highest viscosity of each hydrogel represents the point where the solid-like elastic state breaks down and transforms to a fluid-like state. The HA-Alg (5:5) hydrogel exhibited a higher viscosity (30.4 ± 0.83 Pa.s) compared to the HA-Alg-SF hydrogel (12.6 ± 1.27 Pa.s). A decrease in viscosity was observed at shear rates higher than 9.1 s^{-1} in HA-Alg (5:5) hydrogel and higher than 6.6 s^{-1} in HA-Alg-SF hydrogel, indicating their remarkable shear-thinning behaviour. The shear-thinning properties of both hydrogels indicated that they readily passed through the nozzle during printing process, while retaining the gel state after extruding [40,41]. Correspondingly, the shear stress (τ) applied on HA-Alg (5:5) and HA-Alg-SF hydrogels in this model was determined by the relationship between apparent viscosity (η) and shear rate (γ), as follows

$$\tau = \eta\gamma$$

The shear stress at maximum viscosity of HA-Alg (5:5) and HA-Alg-SF hydrogels were 276.6 Pa and 83.2 Pa, respectively. A high shear

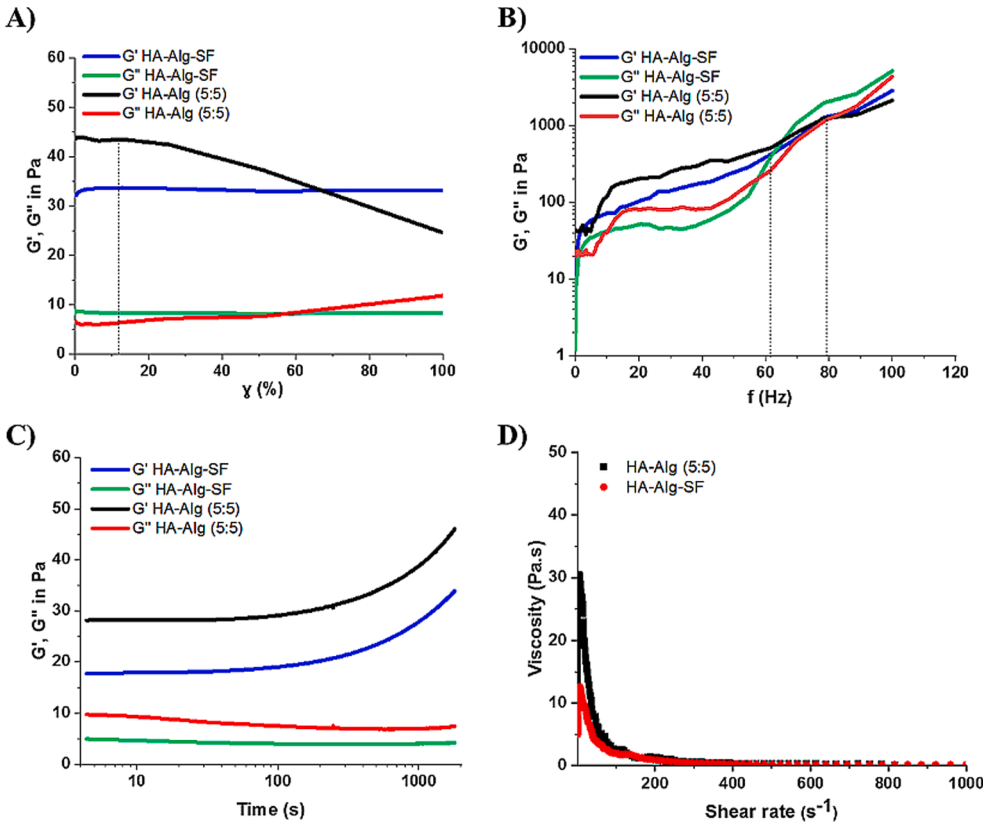

Fig. 8. Rheological analysis of HA-Alg (5:5) and HA-Alg-SF hydrogels. (A) Strain sweep, (B) Frequency sweep, (C) Time sweep, and (D) Shear-thinning behaviour.

stress can affect both cell viability and cell proliferation. It was reported in previous research that a high cell viability was maintained in 3D printing if a shear stress lower than 5 kPa was applied [42–44]. The data in rheological analysis and cell viability after printing (Fig. 6C) suggested that the viscosity and shear stress of both hydrogels were within acceptable ranges for printing cells using our custom-made 3D bioprinter (Enterprise 2.0).

3.8. In vitro cytocompatibility of HA-Alg (5:5) and HA-Alg-SF hydrogels

An assessment of cytotoxicity and cell distribution was performed using a LIVE/DEAD cell viability assay on day 1, 3 and 7 post-encapsulation. hMSCs showed a homogeneous distribution in HA-Alg (5:5) and HA-Alg-SF hydrogels (Fig. 9A). The DNA content of both hydrogels slightly increased for up to 7 days, including the DNA content of the fibrin control group (Fig. 9B) [24]. In addition, immunohistochemistry of Ki-67, the protein in active phases of the cell cycle G1, S, G2 and mitosis, was detected in the HA-Alg (5:5) and HA-Alg-SF hydrogels (Supplementary Fig. S2). The cytotoxicity of both hydrogels was investigated using PrestoBlue™ assay (Fig. 9C). The fluorescent values corresponded with resorufin, a red fluorescent compound generated from the mitochondrial reductase enzyme of active cells, which reflects cellular metabolism [45]. Both hydrogels showed an increase in fluorescence unit throughout the 7-day culture period, indicating the non-toxicity of hydrogel against hMSCs. These studies demonstrated that HA-Alg (5:5) and HA-Alg-SF hydrogels supported cell proliferation without cytotoxicity.

3.9. Chondrogenic differentiation of hMSCs and cartilage tissue formation

hMSCs were encapsulated into HA-Alg (5:5) and HA-Alg-SF hydrogels and cultured in chondrogenic medium. The cell-seeded hydrogels were stiff and progressed to opaque constructs over week 4 of culture (Fig. 10A), suggesting that chondrogenic differentiation of hMSCs occurred and the cells laid down an extracellular matrix within the hydrogels. To confirm the presence of cartilaginous matrix, type II collagen fluorescent staining was detected in both constructs in a higher abundance on week 4 compared to week 2 (Fig. 10B). The secretion of glycosaminoglycans (GAGs), which is also a chondrogenic marker, was found in both HA-Alg (5:5) and HA-Alg-SF after week 2 and week 4 by Alcian Blue staining (Fig. S3). Corresponding with the cytocompatibility results, HA-Alg (5:5) and HA-Alg-SF hydrogels exhibited an excellent supporting biomaterial for the chondrogenic differentiation of hMSCs, providing an alternative option for the regeneration of cartilage tissue.

4. Discussion

Hydrogel is commonly used as a bioink because of its hydrated environment, which is similar to native tissue, excellent biocompatibility and adjustable viscosity. The viscosity of hydrogels was influenced by several parameters, including the chemical composition of hydrogels, concentrations of polymers and temperature that allow for shear-thinning properties to occur during hydrogel ejected from a 3D bioprinter nozzle. Modulating viscosity is a key to control the gelation process, which ultimately facilitates 3D bioprinting technology [7,9,46–48].

In this study, we aimed to develop the hydrogel, comprising bacterial HA and Alg, which is intended for use as a bioink. The gelation of the HA-Alg hydrogel was induced by covalent crosslinking via imine bonds, which was self-healing, temperature-independent and demonstrated competitive advantages over other options for material handling.

HA provides a biological cue in the HA-Alg hydrogel system, as one of the principle extracellular matrix components [17,49–51]. However,

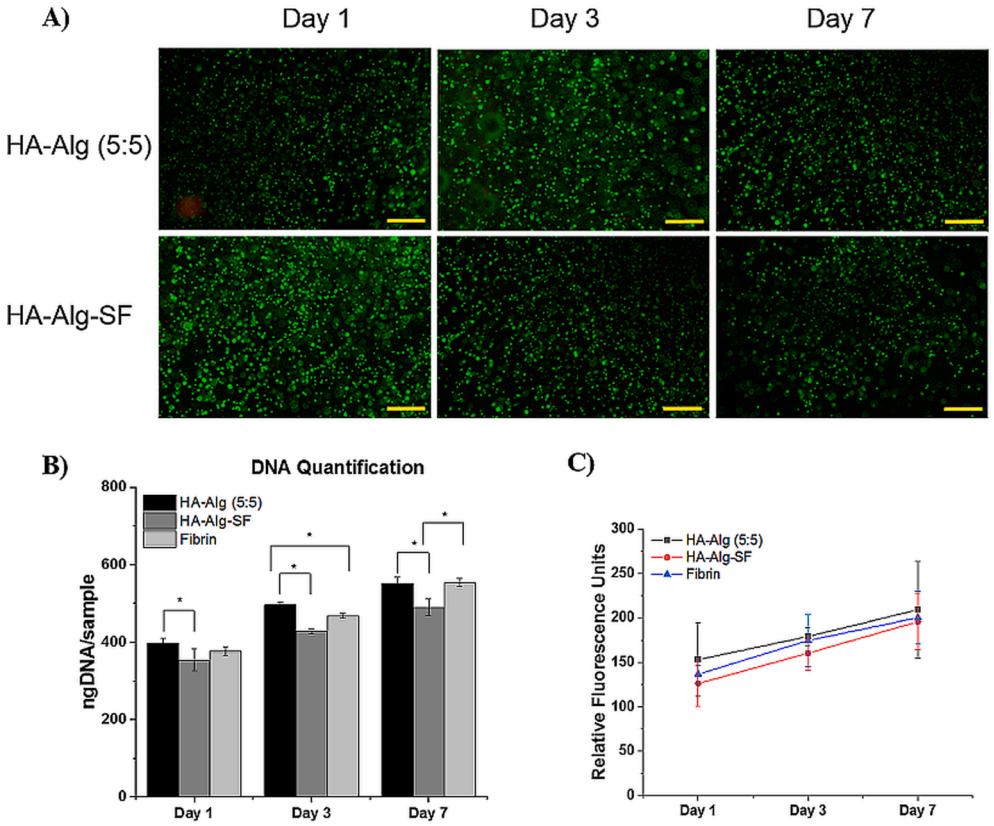

Fig. 9. In vitro cytocompatibility of HA-Alg (5:5) and HA-Alg-SF hydrogels. (A) Live/Dead staining of hMSCs encapsulated in hydrogels on day 1, 3 and 7, (scale bars: 500 μm), (B) Quant-i™ Picogreen™ dsDNA Assay. Asterisk (*) represents significant difference between samples ($p < 0.05$), and (C) PrestoBlue™ assay.

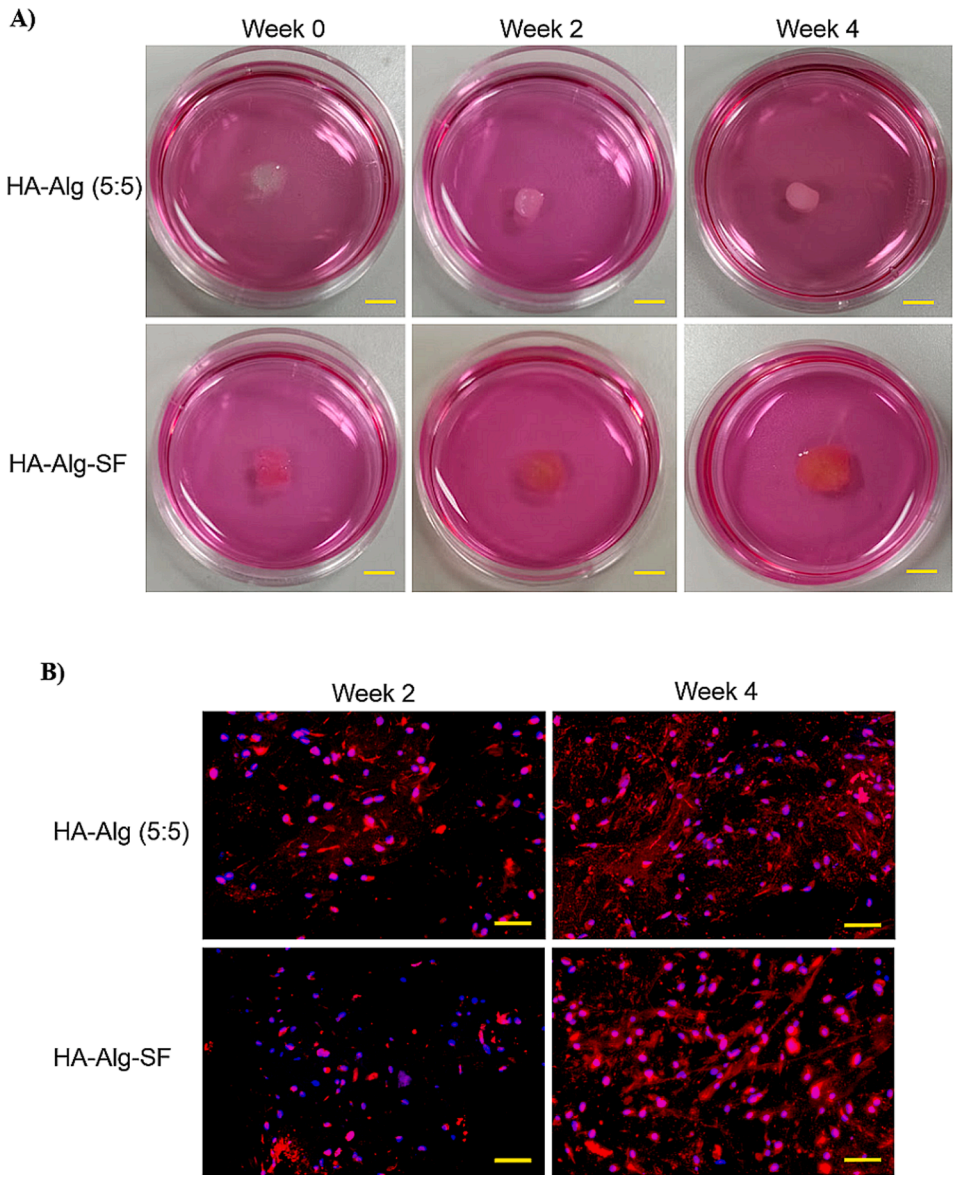

Fig. 10. Cartilage tissue formation. (A) hMSCs encapsulated in hydrogels for 0, 2 and 4 weeks (scale bars: 5 mm), and (B) Immunofluorescent staining of type II collagen in hydrogel constructs after 2 weeks and 4 weeks (scale bars: 200 μm), red: type II collagen, blue: cell nuclei. (For interpretation of the references to colour in this figure legend, the reader is referred to the web version of this article.)

it is difficult to form gel alone because of low mechanical properties and rapid degradation. To leverage the use of HA in tissue-engineering applications and bioink, gelling agents are needed to improve the structural stability of HA. Alg has been reported as a biopolymer with high mechanical stiffness and slow degradation, providing great benefits for the long-term culture of bone and cartilage tissue [52]. Most studies, HA and Alg were ionic crosslinked using Ca^{2+}. The rapid gelation of this HA-Alg hydrogel has been difficult to control and limited in printability [52,53]. HA and Alg were chemically modified to conjugate amino (—NH_2) and aldehyde (—CHO) groups into their polymeric structures. The carboxyl groups (—COOH) on HA molecules were activated by EDC/HOBt to conjugate with ethylenediamine. For Alg, the modification was based on the oxidation at carbon atoms (C-2 and C-3) on alginitic polymeric subunits. After breaking the bond between C-2 and C-3, 2 aldehyde functional groups were formed.

Crosslinking between HA-NH_2 and Alg-CHO resulted from Schiff's base reaction. The success in the chemical modification of HA and Alg and creation of the HA-Alg hydrogel was confirmed by NMR and FTIR. The HA-Alg hydrogel with tuneable properties, by varying volume ratios of HA-NH_2 and Alg-CHO, could expand the range of applications to encapsulate different cell types and differentiate specific tissues.

During the fabrication process, three volume ratios of HA-NH_2 and Alg-CHO of 5:5, 6:4 and 7:3 were able to form hydrogels (Table 1 and Fig. 4). The HA-Alg (5:5) hydrogels were more rigid than the HA-Alg hydrogels at other volume ratios, both 6:4 and 7:3. The slow degradation of HA-Alg (5:5) hydrogel goes in line with the gelation outcomes. The HA-Alg (5:5) hydrogel remained intact in PBS solution for up to 40 days, while hydrogels at other ratios showed significant weight loss: 95.4 ± 8.0 % in HA-Alg (6:4) hydrogel and 89.4 ± 5.3% in HA-Alg hydrogel (7:3) (Supplementary Table S1).

The HA-Alg (5:5) hydrogel was investigated as a potential bioink with extrusion-based printability, a cell encapsulation matrix, mechanical properties, cytocompatibility and cartilage tissue formation. All studies of the HA-Alg (5:5) hydrogel were carried out in parallel with the entrapment of silk fibroin (SF) to evaluate the IPN's capabilities of the HA-Alg (5:5) hydrogel. SF, a polypeptide from *Bombyx mori* silkworms, was mixed with HA-NH_2 first to prevent the crosslinking between amino groups on SF and aldehyde groups on Alg-CHO. Interestingly, the

addition of SF could minimize weight loss in the hydrogel constructs more than HA-Alg (6:4) and HA-Alg (7:3) in Fig. 4. This clearly showed that HA-Alg (6:4) and HA-Alg (7:3) hydrogels had greater weight loss than the HA-Alg (5:5), with and without SF. Further investigations are necessary to clearly understand if SF, HA or Alg still remain in the cell-loaded constructs.

Incorporating SF into the HA-Alg hydrogel did not affect 3D bioprintability and hMSC viability. The HA-Alg (5:5) hydrogel can precisely print grid patterns better than that with SF (Fig. 6D). The higher spatial resolution of printed HA-Alg (5:5) hydrogel compared to HA-Alg-SF hydrogel could be explained by the 2.4-times higher viscosity of HA-Alg (5:5) hydrogel compared to HA-Alg-SF hydrogel, suggesting that SF possibly interfered the HA-Alg network. To improve the viscosity of HA-Alg-SF hydrogel, increasing the degree of crosslinking might reinforce the HA-Alg hydrogel network and improve shear-thinning of the hydrogel that is incorporated with other polymeric molecules, and not limited to SF. However, it is interesting to note that bulk mechanical properties of HA-Alg (5:5) and HA-Alg-SF did not show significant differences, as demonstrated by their similar compressive and elastic moduli (Fig. 7). Both HA-Alg (5:5) and HA-Alg-SF hydrogels exhibited elastic behaviours ($G' > G''$), and could be quickly prepared for 3D bioprinting, without compromising homogenous cell distribution.

Moreover, important biological properties of HA-Alg (5:5) and HA-Alg-SF hydrogels were confirmed by several assays (LIVE/DEAD® Kit, Quant-iT™ Picogreen™ dsDNA and PrestoBlue™). Cell proliferation marker in the tissue constructs HA-Alg (5:5) and HA-Alg-SF increased through culture time and was more prominent in HA-Alg (5:5), particularly for DNA content from day 7 onwards.

As it was more relevant than monolayer cell culture, the fibrin hydrogel [23] was used as the control group to assess the cartilage tissue development in HA-Alg (5:5) and HA-Alg-SF hydrogels. We demonstrated that hMSCs encapsulated in HA-Alg (5:5) and HA-Alg-SF could transform hydrogel from a transparent to opaque construct in 4 weeks. Cartilaginous matrix production by hMSCs was confirmed by type II collagen and GAGs staining in both hydrogels. Assessing the biomechanical properties of the tissue constructs will be necessary to evaluate the progression of compressive strength and elastic modulus.

Animal-free and plant-based smart biomaterials are an emerging field in tissue engineering [54,55]. To create engineered tissue, in vitro tissue constructs were originally generated using a top-down approach, such as casting cell-laden hydrogels or seeding cells into pre-made porous scaffolds. Currently, the bottom-up approach can fabricate tissue constructs lay-by-layer using 3D bioprinting. The biomaterials used in this study were bacterial- and algae-derived hydrogels. We demonstrated the lab-grown cartilage was created by the top-down approach, while cell viability was demonstrated in a short-term culture using the bottom-up approach by 3D bioprinting. Our workflow was divided into three phases. Firstly, the hydrogel was developed as an IPN platform and printability was tested (hydrogel and 3D bioprinter). Secondly, the hydrogel was investigated biocompatibility and tissue development (hydrogel and cells). Finally, printing cell-laden hydrogel was conducted to demonstrate homogenous cell distribution printed in grid pattern (cells, hydrogel, and 3D bioprinter), which was not intended for long-term culture.

5. Conclusion

This study reports on a novel composite hydrogel made from HA-NH_2 and Alg-CHO. To initiate the gelation process, HA-NH_2 was crosslinked with Alg-CHO with different volume ratios, resulting in the formation of imine bonds (C═N). The HA-Alg hydrogel with volume ratios of 5:5 exhibited a matrix capable of supporting cartilage tissue formation. The versatility of the HA-Alg (5:5) hydrogel was demonstrated by tailoring its mechanical properties, degradation time, and viscosity. Shear-thinning behaviour and consistent biological properties (cell viability/proliferation) of the HA-Alg (5:5) hydrogel suggested that these key features contribute to extrusion-based 3D bioprinting technology. Finally, the HA-Alg (5:5) hydrogel demonstrated an IPN, which could facilitate the development of a versatile platform to entangle other macromolecules such as silk fibroin as shown herein.

Funding

We gratefully acknowledge the research funding received from the graduate scholarship programme for ASEAN Countries, Chulalongkorn University (to T.N.T); Ratchadapiseksompotch Fund, Faculty of Medicine, Chulalongkorn University (grant number RA60/116 to S.Y.); PMUC (grant number C10F640050 to S.Y.).

CRediT authorship contribution statement

Truc Nguyen Thanh: Methodology, Visualization, Writing – original draft. **Navaporn Laowattanatham:** Software, Validation. **Juthamas Ratanavaraporn:** Resources. **Amornpun Sereemaspun:** Funding acquisition. **Supansa Yodmuang:** Conceptualization, Investigation, Writing – review & editing.

Declaration of Competing Interest

The authors declare the following financial interests/personal relationships which may be considered as potential competing interests: T. N.T and S.Y. are named inventors in the patent application related to the HA-Alg hydrogel and bioink. N.L. is a co-founder of the Winner prototype, a 3D printer start-up. Other co-authors do not have conflicts to declare.

Acknowledgements

We acknowledge the assistance and support of the Scientific and Technological Research Equipment Centre, Chulalongkorn University. We also acknowledge Pensuda Sompunga for her help with hydrogel preparation, Dr. Jittima Luckanagul for rheology analysis, and Dr. Depicha Jindatip for histological study. The authors would like to thank Dr. Joao Nuno Andrade Requicha Ferreira for proofreading the manuscript.

Data availability

The raw/processed data required to reproduce these findings cannot be shared at this time as the data also forms part of an ongoing study.

Appendix A. Supplementary material

Supplementary data to this article can be found online at https://doi.org/10.1016/j.eurpolymj.2022.111027.

References

[1] Y. Kanno, T. Nakatsuka, H. Saijo, Y. Fujihara, H. Atsuhiko, U.-i. Chung, T. Takato, K. Hoshi, Computed tomographic evaluation of novel custom-made artificial bones, "CT-bone", applied for maxillofacial reconstruction, Regenerative Therapy 5 (2016) 1–8.
[2] L. Roseti, C. Cavallo, G. Desando, V. Parisi, M. Petretta, I. Bartolotti, B. Grigolo, Three-Dimensional Bioprinting of Cartilage by the Use of Stem Cells: A Strategy to Improve Regeneration, Materials (Basel, Switzerland) 11 (9) (2018) 1749, https://doi.org/10.3390/ma11091749.
[3] M. Javaid, A. Haleem, 3D bioprinting applications for the printing of skin: A brief study, Sens. Int. 2 (2021), 100123.
[4] J.H. Galarraga, M.Y. Kwon, J.A. Burdick, 3D bioprinting via an in situ crosslinking technique towards engineering cartilage tissue, Sci. Rep. 9 (1) (2019) 19987.
[5] J. Gopinathan, I. Noh, Recent trends in bioinks for 3D printing, Biomater. Res. 22 (2018), 11–11.
[6] P.S. Gungor-Ozkerim, I. Inci, Y.S. Zhang, A. Khademhosseini, M.R. Dokmeci, Bioinks for 3D bioprinting: an overview, Biomater. Sci. 6 (5) (2018) 915–946.

[7] P. Ramiah, L.C. du Toit, Y.E. Choonara, P.P.D. Kondiah, V. Pillay, Hydrogel-Based Bioinks for 3D Bioprinting in Tissue Regeneration, Front. Mater. 7 (2020), https://doi.org/10.3389/fmats.2020.00076.

[8] H. Li, C. Tan, L. Li, Review of 3D printable hydrogels and constructs, Mater. Des. 159 (2018) 20–38.

[9] J.M. Unagolla, A.C. Jayasuriya, Hydrogel-based 3D bioprinting: A comprehensive review on cell-laden hydrogels, bioink formulations, and future perspectives, Appl. Mater. Today 18 (2020), 100479.

[10] C. Antich, J. de Vicente, G. Jiménez, C. Chocarro, E. Carrillo, E. Montañez, P. Gálvez-Martín, J.A. Marchal, Bio-inspired hydrogel composed of hyaluronic acid and alginate as a potential bioink for 3D bioprinting of articular cartilage engineering constructs, Acta Biomater. 106 (2020) 114–123.

[11] I. Noh, N. Kim, H.N. Tran, J. Lee, C. Lee, 3D printable hyaluronic acid-based hydrogel for its potential application as a bioink in tissue engineering, Biomater. Res. 23 (1) (2019), https://doi.org/10.1186/s40824-018-0152-8.

[12] J.-W. Kuo, G.D. Prestwich, in: Comprehensive Biomaterials, Elsevier, 2011, pp. 239–259, https://doi.org/10.1016/B978-0-08-055294-1.00073-8.

[13] S.A. Unterman, M. Gibson, J.H. Lee, J. Crist, T. Chansakul, E.C. Yang, J.H. Elisseeff, Hyaluronic acid-binding scaffold for articular cartilage repair, Tissue Eng. Part A 18 (23-24) (2012) 2497–2506.

[14] A.M. Patti, A. Gabriele, A. Vulcano, M.T. Ramieri, C. Della Rocca, Effect of hyaluronic acid on human chondrocyte cell lines from articular cartilage, Tissue Cell 33 (3) (2001) 294–300.

[15] D.H. Manicourt, J.C. Pita, Quantification and Characterization of Hyaluronic Acid in Different Topographical Areas of Normal Articular Cartilage from Dogs, Collagen Related Res. 8 (1) (1988) 39–47.

[16] C. Pfeifer, A. Berner, M. Koch, W. Krutsch, R. Kujat, P. Angele, M. Nerlich, J. Zellner, Higher Ratios of Hyaluronic Acid Enhance Chondrogenic Differentiation of Human MSCs in a Hyaluronic Acid-Gelatin Composite Scaffold, Materials (Basel, Switzerland) 9 (5) (2016) 381, https://doi.org/10.3390/ma9050381.

[17] A. Gilarska, J. Lewandowska-Łańcucka, W. Horak, M. Nowakowska, Collagen/chitosan/hyaluronic acid – based injectable hydrogels for tissue engineering applications – design, physicochemical and biological characterization, Colloids Surf., B 170 (2018) 152–162.

[18] L.-S. Kontturi, E. Järvinen, V. Muhonen, E.C. Collin, A.S. Pandit, I. Kiviranta, M. Yliperttula, A. Urtti, An injectable, in situ forming type II collagen/hyaluronic acid hydrogel vehicle for chondrocyte delivery in cartilage tissue engineering, Drug Deliv. Transl. Res. 4 (2) (2014) 149–158.

[19] K.Y. Lee, D.J. Mooney, Alginate: properties and biomedical applications, Prog. Polym. Sci. 37 (1) (2012) 106–126.

[20] V.S. Ghorpade, Chapter 4 - Preparation of hydrogels based on natural polymers via chemical reaction and cross-Linking, in: Y. Chen (Ed.), Hydrogels Based on Natural Polymers, Elsevier, 2020, pp. 91–118.

[21] H. Tan, H. Li, J.P. Rubin, K.G. Marra, Controlled gelation and degradation rates of injectable hyaluronic acid-based hydrogels through a double crosslinking strategy, J. Tissue Eng. Regener. Med. 5 (10) (2011) 790–797.

[22] C. Laomeephol, M. Guedes, H. Ferreira, R.L. Reis, S. Kanokpanont, S. Damrongsakkul, N.M. Neves, Phospholipid-induced silk fibroin hydrogels and their potential as cell carriers for tissue regeneration, J. Tissue Eng. Regener. Med. 14 (1) (2020) 160–172.

[23] T.T. Nguyễn, J. Ratanavaraporn, S. Yodmuang, Alginate-silk fibroin Bioink : A printable hydrogel for tissue engineering. 2019 12th Biomedical Engineering International Conference (BMEiCON), 2019.

[24] H.-W. Kang, et al., A 3D bioprinting system to produce human-scale tissue constructs with structural integrity, Nat. Biotechnol. 34 (2016) 312.

[25] I. Youm, V. Agrahari, J.B. Murowchick, B.-B. Youan, Uptake and Cytotoxicity of Docetaxel-Loaded Hyaluronic Acid-Grafted Oily Core Nanocapsules in MDA-MB 231 Cancer Cells, Pharm. Res. 31 (9) (2014) 2439–2452.

[26] T. Snyder, et al., Erratum to: A fibrin/hyaluronic acid hydrogel for the delivery of mesenchymal stem cells and potential for articular cartilage repair, J. Biol. Eng. 8 (2014) 10.

[27] L. Wang, Y. Wang, J. Hao, S. Dong, Magnetic Fullerene-DNA/Hyaluronic Acid Nanovehicles with Magnetism/Reduction Dual-Responsive Triggered Release, Magnetic Fullerene-DNA/Hyaluronic Acid Nanovehicles with Magnetism/Reduction Dual-Responsive Triggered Release 18 (3) (2017) 1029–1038.

[28] T. Salomonsen, et al., Rapid Determination of Alginate Monomer Compostion using Raman Spectroscopy and Chemometrics, in: Gums and Stabilisers for the Food Industry 14, The Royal Society of Chemistry, 2008, pp. 543–551.

[29] L. Wang, Y. Hou, X. Zhong, J. Hu, F. Shi, H. Mi, Preparation and catalytic performance of alginate-based Schiff Base, Carbohydr. Polym. 208 (2019) 42–49.

[30] A. Usov, M. Bilan, N.G. Klochkova, Polysaccharides of Algae. 48. Polysaccharide Composition of Several Calcareous Red Algae: Isolation of Alginate from Corallina pilulifera P. et R. (Rhodophyta, Corallinaceae), 1995.

[31] S. Mallakpour, A. Zadehnazari, Synthesis, morphology investigation and thermal mechanical properties of dopamine-functionalized multi-walled carbon nanotube/poly(amide-imide) composites, React. Funct. Polym. 106 (2016) 112–119.

[32] S.-H. Lee, S.-R. Shin, D.-S. Lee, Self-healing of cross-linked PU via dual-dynamic covalent bonds of a Schiff base from cystine and vanillin, Mater. Des. 172 (2019), 107774.

[33] H. Rahmani, A. Fattahi, K. Sadrjavadi, S. Khaledian, Y. Shokoohinia, Preparation and Characterization of Silk Fibroin Nanoparticles as a Potential Drug Delivery System for 5-Fluorouracil, Adv. Pharm. Bull. 9 (4) (2019) 601–608.

[34] A.R. Murphy, D.L. Kaplan, Biomedical applications of chemically-modified silk fibroin, J. Mater. Chem. 19 (36) (2009) 6443–6450.

[35] Q. Dong, X. Guo, L. Li, C. Yu, L. Nie, W. Tian, H. Zhang, S. Huang, H. Zang, Understanding hyaluronic acid induced variation of water structure by near-infrared spectroscopy, Sci. Rep. 10 (1) (2020), https://doi.org/10.1038/s41598-020-58417-5.

[36] R. Subramani, A. Izquierdo-Alvarez, P. Bhattacharya, M. Meerts, P. Moldenaers, H. Ramon, H. Van Oosterwyck, The Influence of Swelling on Elastic Properties of Polyacrylamide Hydrogels, The Influence of Swelling on Elastic Properties of Polyacrylamide Hydrogels 7 (2020), https://doi.org/10.3389/fmats.2020.0021210.3389/fmats.2020.00212.s001.

[37] M. Klak, P. Kowalska, T. Dobrzański, G. Tymicki, P. Cywoniuk, M. Gomółka, K. Kosowska, T. Bryniarski, A. Berman, A. Dobrzyń, W. Sadowski, B. Górecki, M. Wszoła, Bionic Organs: Shear Forces Reduce Pancreatic Islet and Mammalian Cell Viability during the Process of 3D Bioprinting, Micromachines 12 (3) (2021) 304, https://doi.org/10.3390/mi12030304.

[38] M.H. Amer, L.J. White, K.M. Shakesheff, The effect of injection using narrow-bore needles on mammalian cells: administration and formulation considerations for cell therapies, J. Pharm. Pharmacol. 67 (5) (2015) 640–650.

[39] S. Naghieh, M.D. Sarker, N.K. Sharma, Z. Barhoumi, X. Chen, Printability of 3D Printed Hydrogel Scaffolds: Influence of Hydrogel Composition and Printing Parameters, Appl. Sci. 10 (1) (2020) 292, https://doi.org/10.3390/app10010292.

[40] W. Liu, M.A. Heinrich, Y. Zhou, A. Akpek, N. Hu, X. Liu, X. Guan, Z. Zhong, X. Jin, A. Khademhosseini, Y.S. Zhang, Extrusion Bioprinting of Shear-Thinning Gelatin Methacryloyl Bioinks, Adv. Healthcare Mater. 6 (12) (2017) 1601451, https://doi.org/10.1002/adhm.201601451.

[41] D. Petta, et al., 3D printing of a tyramine hyaluronan derivative with double gelation mechanism for independent tuning of shear thinning and post-printing curing, ACS Biomater. Sci. Eng. 4 (2018).

[42] D. Trucco, A. Sharma, C. Manferdini, E. Gabusi, M. Petretta, G. Desando, L. Ricotti, J. Chakraborty, S. Ghosh, G. Lisignoli, Modeling and Fabrication of Silk Fibroin–Gelatin-Based Constructs Using Extrusion-Based Three-Dimensional Bioprinting, ACS Biomater. Sci. Eng. 7 (7) (2021) 3306–3320.

[43] A. Blaeser, D.F. Duarte Campos, U. Puster, W. Richtering, M.M. Stevens, H. Fischer, Controlling Shear Stress in 3D Bioprinting is a Key Factor to Balance Printing Resolution and Stem Cell Integrity, Adv. Healthc. Mater. 5 (3) (2016) 326–333.

[44] J. Shi, B. Wu, S. Li, J. Song, B. Song, W.F. Lu, Shear stress analysis and its effects on cell viability and cell proliferation in drop-on-demand bioprinting, Biomed. Phys. Eng. Express 4 (4) (2018) 045028, https://doi.org/10.1088/2057-1976/aac946.

[45] N. Lall, et al., Viability Reagent, PrestoBlue, in Comparison with Other Available Reagents, Utilized in Cytotoxicity and Antimicrobial Assays, Int. J. Microbiol. 2013 (2013), 420601–420601.

[46] A. Blaeser, D.F. Duarte Campos, H. Fischer, 3D bioprinting of cell-laden hydrogels for advanced tissue engineering. Current Opinion, Biomed. Eng. 2 (2017) 58–66.

[47] M.M. Stanton, J. Samitier, S. Sánchez, Bioprinting of 3D Hydrogels, Lab Chip 15 (15) (2015) 3111–3115.

[48] X. Wang, et al., Gelatin-Based Hydrogels for Organ 3D Bioprinting, Polymers 9 (2017) 401.

[49] M. Rubert, M. Alonso-Sande, M. Monjo, J.M. Ramis, Evaluation of Alginate and Hyaluronic Acid for Their Use in Bone Tissue Engineering, Biointerphases 7 (1) (2012) 44, https://doi.org/10.1007/s13758-012-0044-8.

[50] M. Müller, E. Öztürk, Ø. Arlov, P. Gatenholm, M. Zenobi-Wong, Alginate Sulfate-Nanocellulose Bioinks for Cartilage Bioprinting Applications, Ann. Biomed. Eng. 45 (1) (2017) 210–223.

[51] Y.P. Singh, A. Bandyopadhyay, B.B. Mandal, 3D Bioprinting Using Cross-Linker-Free Silk-Gelatin Bioink for Cartilage, Tissue Eng. 11 (37) (2019) 33684–33696.

[52] K. Ziv, H. Nuhn, Y. Ben-Haim, L.S. Sasportas, P.J. Kempen, T.P. Niedringhaus, M. Hrynyk, R. Sinclair, A.E. Barron, S.S. Gambhir, A tunable silk–alginate hydrogel scaffold for stem cell culture and transplantation, Biomaterials 35 (12) (2014) 3736–3743.

[53] S.J. Lee, J.M. Seok, J.H. Lee, J. Lee, W.D. Kim, S.A. Park, Three-Dimensional Printable Hydrogel Using a Hyaluronic Acid/Sodium Alginate Bio-Ink, Three-Dimensional Printable Hydrogel Using a Hyaluronic Acid/Sodium Alginate Bio-Ink 13 (5) (2021) 794, https://doi.org/10.3390/polym13050794.

[54] S. Iravani, R.S. Varma, Plants and plant-based polymers as scaffolds for tissue engineering, Green Chem. 21 (18) (2019) 4839–4867.

[55] A. Indurkar, A. Pandit, R. Jain, P. Dandekar, Plant-based biomaterials in tissue engineering, Bioprinting 21 (2021) e00127, https://doi.org/10.1016/j.bprint.2020.e00127.